Block Copolymer Adsorption Studied by Dynamic Scanning Angle Reflectometry

Frans A. M. Leermakers† and Alice P. Gast*

Department of Chemical Engineering, Stanford University, Stanford, California 94305

Received April 23, 1990; Revised Manuscript Received July 26, 1990

ABSTRACT: We employ a novel scanning angle reflectometer to study both the kinetics of block copolymer adsorption and the structure of the adsorbed layer. The apparatus measures the intensity of parallel polarized light reflected from a glass–solution interface at and around the Brewster angle. We study the deposition of highly asymmetric styrene/ethylene oxide (S/EO) block copolymers from cyclopentane. When the surface is challenged with a concentrated or moderately dilute polymer solution, a very fast initial chain deposition is observed. This layer is always far from equilibrium, relaxing slowly over periods of days. Stable layers are prepared by using the concentration step procedure: the initial coverage at extremely low polymer solution concentration allows for individual chain relaxations; subsequent increases in polymer solution concentration result in stable, thicker, polymer layers within 1 h. Such layers are in semiquantitative agreement with those calculated from the self-consistent-field theory due to Scheutjens and Fleer. The computations suggest that at very low concentrations both types of segments can adsorb, while at higher concentrations the EO units displace the PS segments and the characteristic profile of the highly extended "grafted" PS tails is present. Analysis of the adsorption kinetics shows transport of chains through the brush layer to be relatively fast while chain rearrangements in the adsorbed layer are prohibitively slow. At a coverage on the order of 10 mg/m^2, a phase transition in the polymer layer is observed. This new layer has a more compact, less extended structure.

Introduction

Block copolymers have much in common with short-chain surfactants. In a selective solvent they self-assemble above a given concentration (cmc) to form well-defined micellar structures. Due to the cooperative nature of the many repeat units, they are often extremely surface active. If one of the blocks has a segmental adsorption energy comparable to kT, the surface will be covered by a thick polymer layer, even below the cmc. This property makes block copolymers very useful for applications where, for example, colloidal particles need to be stabilized against flocculation or where surfaces are modified to influence adhesion properties.[1]

Macromolecular and normal surfactants typically differ in length by an order of magnitude. The larger size of the copolymers makes them amenable to optical interrogation. Dynamic light scattering provides the hydrodynamic radius of the single chains as well as information about the hydrodynamic radius distribution and shape of the micelles.[2] Static light scattering provides the radius of gyration, the number of chains in a micelle, and the second virial coefficient for the micellar solution.[3] Polymer adsorption can also be studied by optical techniques. Ellipsometry provides a measure of the adsorbed amount and thickness of the polymer layer[4,5] and can be applied to kinetic studies.[6] The surface plasmon technique has been used to study the kinetics of block copolymer adsorption in terms of adsorbed amounts.[7] In our group, a technique to study block copolymer adsorption using multiple total internal reflections has been developed[8,9] wherein adsorption-induced phase shift of the light is measured interferometrically. With this apparatus we studied the initial deposition process of the PS/PEO block copolymer. Since measurements could not be extended to long times, we sought the alternative experiment described in this paper.

We introduce a new optical technique, dynamic scanning angle reflectometry, to study the adsorption of block copolymers from a gently flowing solution. The principle of scanning angle reflectometry has been known for some time,[4] and a prototype of the apparatus was developed by Déjardin and co-workers for the study of protein adsorption.[10-12] The technique relies on the fact that when (in our case visible) light, polarized parallel to the interface, arrives at a sharp, Fresnel, interface at the Brewster angle, no light is reflected; it is entirely refracted. When the interface is not ideally sharp but, for example, covered by an adsorbate, a small amount of light is reflected. Since the relative change in intensity of the reflected light at the Brewster angle is large, its measurement can be very sensitive to adsorption. Measurement of the reflected light, $I(\alpha)$, at and around the Brewster angle, α_B, provides a reciprocal space picture of the polymer density distribution at the interface. While a unique transformation of $I(\alpha)$ into a density profile is not possible, one can test the ability of a theory to fit reflectivity data. Alternatively, one can show that direct inversion of the reflectivity curves can give zero, first, and signal permitting, second moments of the refractive index profile.

Detailed theories for block copolymers at interfaces have recently been developed. Most of the models focus on scaling relations[13-18] to predict, for example, the dependence of the layer thickness on the molecular composition. Scaling theories provide limiting behavior for a variety of problems; however, numerical constants of proportionality are often omitted. While scaling theories predict the shape of the segment density distribution useful for comparison between systems, detailed quantitative predictions of the density profiles of block copolymer layers are obtained only by computational methods. There have been Monte Carlo simulations of grafted polymer layers mimicking the tail region of an infinitely strong anchored copolymer layer.[19] A full analysis of the equilibrium behavior of adsorbed block copolymer adsorption from micellar solutions is, currently, only available via mean-field and lattice approximations.[20,21] A self-consistent-field theory along these lines, developed by Scheutjens and Fleer,[22-24] has

* To whom correspondence should be addressed.
† Current address: Physical and Colloid Chemistry, Agricultural University, Dreyenplein 6, 6703 HB Wageningen, The Netherlands.

0024-9297/91/2224-0718$02.50/0

been applied to a large variety of inhomogeneous polymer systems. In particular, segment distributions are computed. In contrast to short-chain surfactants, where packing restrictions complicate the structures and require more molecular detail,[25] polymer solutions are well modeled with a first-order Markov approximation. In a variety of polymer adsorption problems, the mean-field theory has reproduced small-angle neutron-scattering data.[26] Model calculations for copolymer systems were presented recently,[20,21] however, thus far no attempts to test these lattice results have been reported.

To summarize, there are experimental as well as theoretical advantages to studying block copolymers rather than surfactant systems, especially since block copolymers having very narrow size distributions and a wide variety of block lengths have become available. As we often use the correspondence with surfactant systems to rationalize the behavior of block copolymers, it is now expected that the study of block copolymers can return insights into the complex behavior of surfactants.

The remainder of this paper is divided into the following parts. We discuss scanning angle reflectometry. In the experimental section we describe the experimental details, some theoretical considerations regarding the reflection of light at an ideal interface, and finally the scanning angle reflectometer calibrations. Some aspects and definitions for the self-consistent-field computations conclude the preliminaries. Reflectivity data obtained from two block copolymers differing in composition will be discussed, followed by a discussion of the scanning angle reflectometry results. The stable layers are compared to predictions of the self-consistent-field theory, and we conclude with a summary of our observations. Reflection by isotropic stratified planar layers is described in Appendix A, and a closed set of equations to compute segment distribution functions with the self-consistent-field theory for polymer adsorption appears in Appendix B.

Scanning Angle Reflectometry

Ellipsometry is a well-established means to measure polymer adsorption,[4] relying on the fact that light polarized parallel (p) and perpendicular (s) to the plane of incidence interacts differently with an inhomogeneous refractive index profile. The reflected light intensity is measured for each polarization; from these two data points two parameters can be determined, usually the mean layer thickness and average refractive index.[4] Often, ellipsometry is performed at a fixed angle where computations of the average thickness and adsorbed amount are available.[5] The surface must have a very high refractive index in order to maximize the signal; thus, in practice ellipsometry is often limited to metallic surfaces. The information obtained by ellipsometry can be increased by scanning multiple angles. Kim and co-workers recently reported ellipsometric measurements providing the profile of adsorbed homopolymers.[27] Their angular range was in the proximity of the critical angle, and only static information for the polymer profile was reported.

Déjardin and co-workers based their experiment on the fact that the intensity of p-polarized light reflected near the Brewster angle is very sensitive to details of the molecules at the interface.[10-12] This method is not limited to metallic surfaces but can be employed at a dielectric interface where the refractive index is typically less than 2. Rotating the sample cell and translating the photomultiplier allowed Déjardin and co-workers to measure the relative intensity of reflected light, $R_p(\alpha)$, for various angles α, ranging about 0.5° around the Brewster angle, α_B. These measurements revealed detailed information on the orientation of protein molecules adsorbed on silica from an aqueous solution. Recording a full Fresnel curve required 50 min, limiting their ability to monitor kinetics. Some kinetic information, obtained by recording the reflectivity at a fixed angle, provided adsorption rates; however, the loss of angular information left the adsorption mechanism unknown.

Block copolymer solutions form very thick adsorption layers,[8,9] and the intensity of the reflected light is several orders of magnitude higher than that in the protein study mentioned above. We are therefore able to replace the photomultiplier by a photodiode array. A cylindrical lens focuses the laser beam at the surface, providing a range of angles spanning the Brewster angle. In this configuration the scanning angle reflectometer can be used to measure time-resolved $R_p(\alpha)$, providing the adsorption kinetics and revealing information about the adsorption mechanism.

Table I
Polymer Characteristics

sample i.d.	M_w	M_n/M_w	PEO, wt %	N(EO)	N(S)
P170/1730	$1.87\ 10^5$	1.10	4	170	1730
P83/3470	$3.65\ 10^5$	1.14	1	83	3470

Experimental Section

(A) Materials. We purchased poly(ethylene oxide)/polystyrene from Polymer Laboratories, Inc. Both polymers (referred to by the number of repeat units) are very asymmetric with monomer ratios of 1:10 and 1:40 EO/S for P170/1730 and P83/3470, respectively. In Table I we list the relevant properties. We purchased cyclopentane, refractive index 1.404, and heptane, refractive index 1.388, from Aldrich Chemical Co. The cyclopentane was 95% pure (5% linear pentane and 30 ppm water). The refractive index increment (dn/dc) for P170/1730 is 0.183 mL/g,[8,9] a value very similar to that of homopolymer PS and P83/3470 because of the low ethylene oxide content.

We determine polymer concentrations down to 10^{-5} g/mL spectrophotometrically by monitoring styrene absorption at 260 nm on a HP8452A diode array spectrophotometer. Some of the solutions in these experiments were below 10^{-5} g/mL; consequently, their exact concentrations are not known. Dilute-solution concentrations can be estimated from initial adsorption rates as described below. Losses of polymer due to adsorption on the container walls become significant at very low concentrations. Since both copolymers have a relatively small EO sequence, their cmc is moderately high; the cmc for P170/1730 is near 10^{-4} g/mL,[28] while for the P83/3470, no micelles are detected by dynamic light scattering up to 10^{-2} g/mL.

(B) Scanning Angle Reflectometer. We show a schematic of the scanning angle reflectometer in Figure 1. The light source is a 3-mW linearly polarized He–Ne laser with a wavelength of 632.8 nm. The laser is positioned with its polarization direction parallel to the plane of incidence. A Glan–Thompson polarizer filters the small s component from the laser output. Via a pinhole, introduced to block reflections, the light passes through a planocylindrical lens with a focal length of 25.4 mm. The focal point is in the prism but not necessarily at the reflection surface. In operation, most of the light is transmitted at the interface and travels into the flow cell to be described below. The reflected light exits the prism and passes through a second polarizer to eliminate any s-polarized light before the intensity is measured by a Reticon photodiode array (RL0128S). The distance from the cylindrical lens (via the prism) to the photodiode array, about 20 cm, provides an angular range of 0.8°. Details of the angular calibration will be discussed below. The scanning angle reflectometer is in a light-tight box to prevent interference from room light.

(C) Prism and Flow Cell. The prism provides the adsorption substrate. We have chosen a Schott Glass Technologies, Inc., high refractive index glass, $n_g = 1.9077$ (LaSFN18), to enhance the measurement sensitivity. Cyclopentane has a refractive index

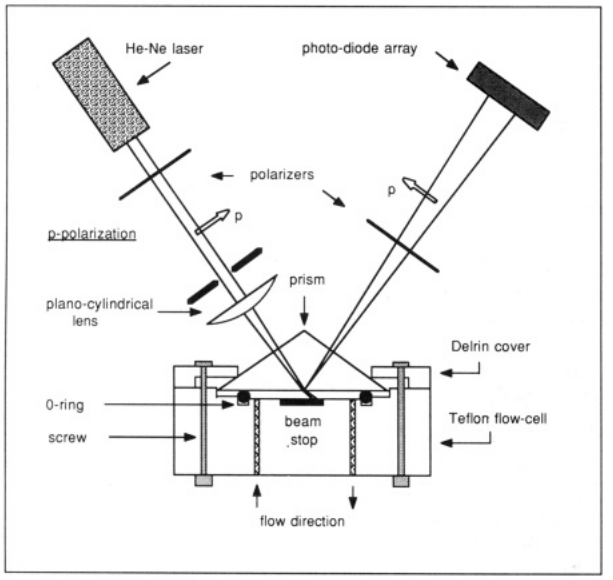

Figure 1. Layout of the scanning angle reflectometer. The key elements of the apparatus are a parallel polarized He–Ne light source, a planocylindrical lens, a glass prism serving as the substrate for adsorption mounted on a flow cell, and a photodiode array detector.

of $n_c = 1.404$, and therefore the Brewster angle defined as $\alpha_B = \arctan(n_c/n_g)$ is 36.37°. The prism dimensions, chosen such that light enters and leaves the prism nearly normal to the glass–air interface to minimize reflections, are 4 cm by 0.5 cm by 1.47 cm high. Three faces of the prism are optically smooth. The prism is mounted on a Teflon flow cell with dimensions 2.5 by 0.5 by 0.1 cm. At the bottom of the flow cell, a neutral density filter, ND3, mounted at a small angle with respect to the incoming beam, deflects reflections away from the photodiode array. The prism is mounted on top of the flow cell by a Delrin cover with an O-ring. We pump the solution at a constant rate, 7.7 mL/min, through the Teflon flow cell with a Fluid Metering, Inc., pump with a FMI pulse dampening system providing a shear rate of approximately 150 s^{-1}. The room temperature was kept at 23 ± 0.5 °C, and the solutions were kept in a water bath at 23 ± 0.1 °C. Temperature variations should not significantly influence the measurements provided the solution temperature remains above or near the Θ temperature of PS in cyclopentane, about 19.5–21.5°.[29]

(D) Data Acquisition and Processing. We began each experiment by cleaning the prism thoroughly with analytical-grade acetone and lens paper until the prism was clean to the eye. Subsequently we subjected the prism to a low-frequency argon plasma cleaner (Harrick Scientific Corp.) for about 20 min. The cleanliness of the substrate, easily examined with the apparatus, was found to be of a consistent quality, although over a period of months a slow increase in surface roughness took place. After mounting the prism and filling the flow system with pure cyclopentane, we found the Brewster angle by visual observation and from the photodiode array signal displayed on an HP54200A digital oscilloscope. A symmetric intensity distribution was proof of alignment.

The measurement was started by flowing a polymer solution through the system. At regular intervals the signal, continuously monitored on the oscilloscope, was stored on a HP 9000/310 computer. During the first 5 min we monitored the profile at 15-s intervals; we lengthened the interval as the processes on the interface slowed. Note that only the intensity of the reflected light relative to the incident light is important. Since the intensity of the laser beam is inhomogeneous (it has an imperfect Gaussian distribution), the laser profile was recorded after each experiment in the same experimental geometry. To do this, the solution was removed from the flow cell so that an interface between polymer-coated glass and air remained. In this geometry the critical angle is superseded, and all light reflects from the interface. This light, attenuated by a neutral density filter, ND3, provided $I_0(\alpha)$. The relative intensity of the reflected light was

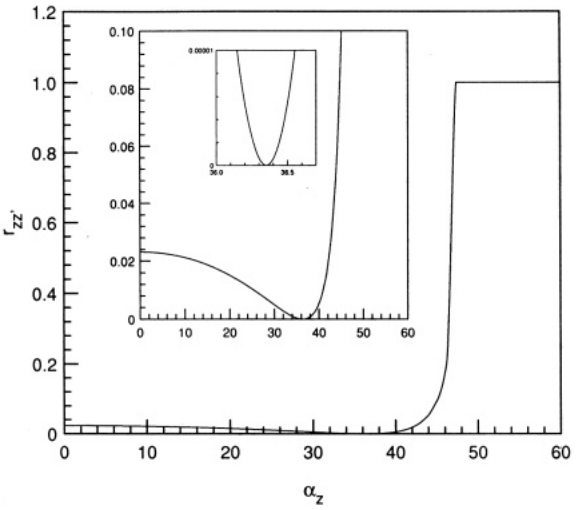

Figure 2. Reflection coefficient, $r_{zz'}$, as a function of incident angle, α_z. The glass has a refractive index $n_0 = 1.907\,73$ and the solution has a refractive index $n_1 = 1.404$. The relevant part of the curve is expanded in the insets.

calculated by $R_p'(\alpha) = I_p(\alpha)/I_0(\alpha)$ and digitally postprocessed to $R_p(\alpha)$. In this process we correct for the introduction of the ND3 neutral density filter. In addition, a smaller but significant correction is needed to account for the slight phase shift upon total reflection of the laser light, which causes a reduction in intensity of the reflected light upon passing through the second polarizer. The total attenuation factor, K, was found by comparing the theoretical Fresnel curve, $R_p^{TFC}(\alpha)$, to the reflectivity curve, $R_p''(\alpha)$ with pure cyclopentane in the flow cell:

$$K = \frac{\int_{\alpha_{min}}^{\alpha_{max}} R_p''(\alpha) - R_p''(\alpha_B)\,d\alpha}{\int_{\alpha_{min}}^{\alpha_{max}} R_p^{TFC}(\alpha)\,d\alpha} \tag{1}$$

The correction factor K, assumed to be independent of angle ($R_p(\alpha) = KR_p'(\alpha)$ for all α), accounts for losses in the optical components and the nonideality of the detection system. Further data processing, for example, the conversion from channel number to angle of incidence, was performed on a SUN 3/260 workstation.

(E) Reflectivity of a Step Profile in Refractive Index. There is considerable literature on the computation of reflectivity from an interface.[4] In Appendix A we summarize the method due to Abelès employing 2 × 2 matrices to compute the reflectivity of a multilayered refractive index profile. This method is well-suited to converting the calculated segment volume fraction profiles obtained from the self-consistent-field theory into a reflectivity curve. Here we focus on the simplest case of a single stratified layer with thickness d_1 and refractive index n_1 in order to give a qualitative picture of the way the reflectivity changes when the interface is modified. Let n_0 and n_2 be the refractive indices of the glass and solvent, respectively. The Fresnel reflection[4]

$$r_{zz'} = \frac{\tan(\alpha_z - \alpha_{z'})}{\tan(\alpha_z + \alpha_{z'})} \tag{2}$$

of parallel polarized light interacting at each interface between two media z and z' depends on the angles of incidence, α_z, and refraction, $\alpha_{z'}$, with respect to the interface normal. In Figure 2 we illustrate the dependence of $r_{zz'}$ on the angle α_z. The film phase thickness[4]

$$\beta_1 = 2\pi\left(\frac{d_1}{\lambda}\right) n_1 \cos\alpha_1 \tag{3}$$

depends on the wavelength of the light, λ, and its path length through the layer. Now the intensity of the reflected parallel

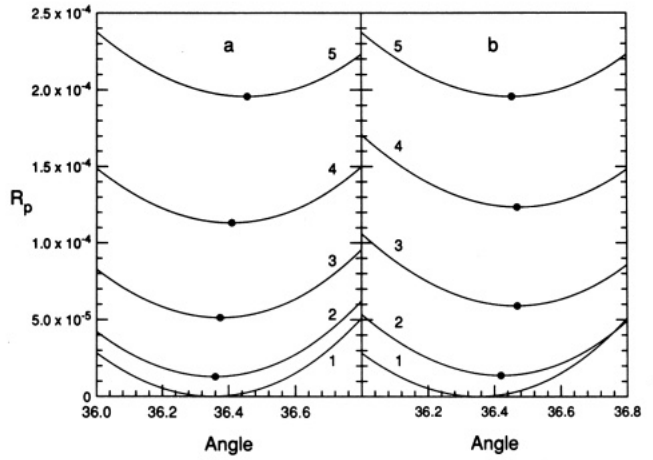

Figure 3. Intensity of the reflected light as a function of incident angle for a theoretical single-step refraction index profile: n_0 = 1.907 73, n_2 = 1.404 (a) at constant refractive index n_1 = 1.5 for (1) d_1 = 0 nm, (2) d_1 = 10 nm, (3) d_1 = 20 nm, (4) d_1 = 30 nm, and (5) d_1 = 40 nm and (b) for a constant thickness d_1 = 40 nm for (1) n_1 = 1.404, (2) n_1 = 1.425, (3) n_1 = 1.45, (4) n_1 = 1.475, and (5) n_1 = 1.5. The points mark the apparent Brewster angles.

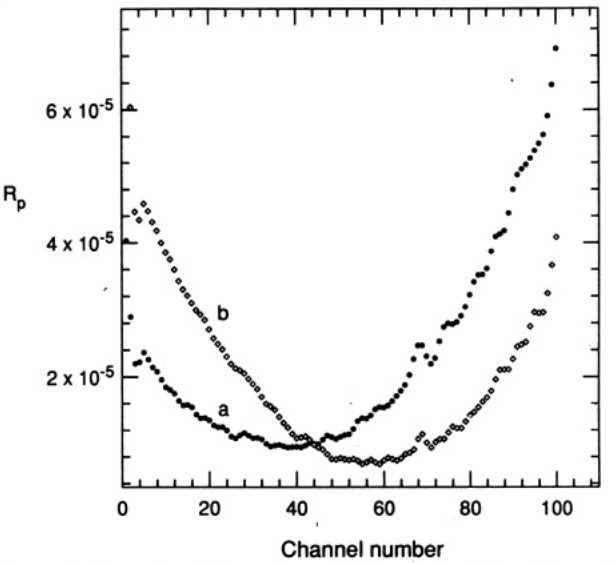

Figure 4. Intensity of the reflected light as a function of channel number for (a) pure cyclopentane and (b) a 50 vol % mixture of cyclopentane and heptane, for a glass surface with refractive index 1.9077.

polarized light relative to that of the incident beam becomes[4]

$$R_p = \frac{r_{01} + r_{12}e^{-j(2\beta_1)}}{1 + r_{01}r_{12}e^{-j(2\beta_1)}} \tag{4}$$

an expression reducing $R_p = r_{01}$ for a film of zero thickness. In this case, when $\alpha_0 - \alpha_1$ equals 90°, the reflected light intensity is zero. This condition defines the Brewster angle. Around this angle we have a nonzero reflected light intensity.

When a layer is present, Déjardin and co-workers showed[11] that, to first approximation, the intensity at the initial Brewster angle is proportional to $R_p(\alpha_B) \sim ((n_1 - n_2)d_1)^2$. Realizing that the product $(n_1 - n_2)d_1$ is proportional to the adsorbed amount, we see that the method is very sensitive to the number of chains at the interface. In general, an increase in intensity of the reflected light at the Brewster angle is accompanied by a shift of the minimum to a higher or lower apparent Brewster angle, $\alpha_{B'}$. This shift generally depends on the adsorbed amount and the refractive index profile of the molecules at the interface. In Figure 3a,b we illustrate the evolution of the Fresnel curve when, at constant refractive index, the layer thickness is changed and when d_1 is fixed and n_1 is modified. This figure shows that an angular shift in the Fresnel curve is indicative of a thickening layer, while an increase in layer refractive index intensity is manifest primarily in increasing intensity.

It must be noted that an ideal Fresnel curve, where the intensity at the Brewster angle is identically zero, only occurs when the interface is represented by a step function in refractive index. Due to surface roughness and impurities, there will always be a finite interfacial width and consequently the reflected light intensity at the Brewster angle is finite.

(F) Calibration. We calibrate our angular resolution (around α_B) by flowing solvents with known refractive index through the system. We follow a pure cyclopentane solution with a mixture of 50 vol % cyclopentane and 50 vol % heptane. The measured refractive index difference between the two solutions, 0.0083, is within the experimental error of the known refractive indices. The distance between the minima in the reflectivity curves (see Figure 4) is 19 channel numbers providing a range for the scanning angle reflectometer photodiode array of 0.8 ± 0.03°. When the Brewster angle (36.4) is exactly at the center of the curve, an angular range from 36.0 to 36.8° is monitored.

Self-Consistent-Field Theory

Without repeating the details of the equilibrium computations for chain molecules in inhomogeneous systems, the ideas and definitions used in the model will be presented here to provide basic insight. We refer to the original papers on this subject[20-24] for a more complete discussion.

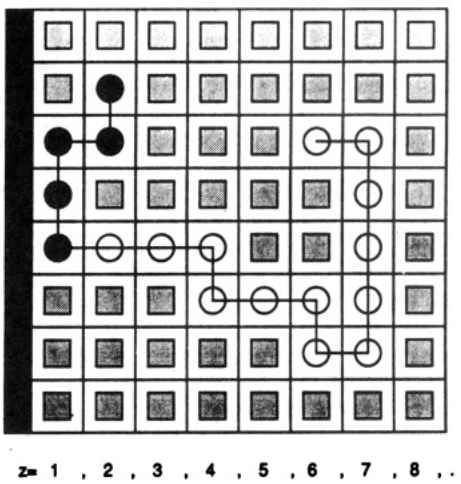

Figure 5. Two-dimensional representation of the lattice in the self-consistent-field computations. The solid wall is indicated ($z < 1$), and lattice layers are numbered $z = 1, ..., M$. A copolymer molecule is shown with a molecular composition A_5B_{13} (A = closed spheres, B = open spheres). Solvent molecules are indicated by filled squares. The polymer volume fraction at layer 2 is $\phi_1(2) = {}^3/_8$ because $\phi_A(2) = {}^2/_8$ and $\phi_B(2) = {}^1/_8$.

In order to count the possible conformations of chain molecules, a lattice is created, as illustrated in two dimensions in Figure 5, where a single block copolymer is near a solid surface and surrounded by solvent monomers. Several approximations made in the theory are directly coupled to the use of such a lattice. One consequence of the lattice is that each site must be filled by either a chain segment or a solvent molecule with all species similar in size. Parallel to the surface we define planar layers numbered $z = 1, ..., M$, each having L lattice sites. A mean-field approximation enables the computation of segmental volume fractions, $\phi_k(z,s)$, in each layer z, for each segment $s = 1, ..., r_k$ of chain type k. Obviously, when the chain length is unity, $r_k = 1$, the molecule k is a monomer. A polymer molecule can have more than one type of segment along its chain; when grouped in blocks these segments correspond to block copolymers. Segment

Table II
Parameters for the SCF Computations[a]

lattice type	hexagonal
no. of segments in statistical unit	5
length of a statistical segment = lattice size	1.2 nm*
dn/dc	0.183 mL/g
$dc/d\phi$	1.675 g/mL*
χ_{WS}	1.25*
χ_{WE}	3.15*
χ_{CE}	1.4
χ_{CS}	0.45
χ_{SE}	0.5
P170/1730	$E_{34}S_{340}$
P83/3470	$E_{17}S_{680}$

[a] An asterisk indicates that the parameter was adjusted to some extent to fit the theory with the experiments.

types are indicated by sub indices x = A, B, C, ..., etc. The layer M is far enough from the surface so that the density profiles have relaxed to the bulk densities of each component (indicated by a super index b). When the density profiles are known, the excess chains of type k adsorbed per surface lattice site can be calculated from

$$\theta_k^{\sigma} = \sum_{s=1}^{r}\sum_{z=1}^{M}(\phi_k(z,s) - \phi_k^{b}) \qquad (5)$$

thus providing the adsorption isotherm $\theta_k^{\sigma}(\phi_k^{b})$. A closed set of equations to calculate the volume fraction of any segment s in a layer z is presented in Appendix B. In addition to the molecular architecture, the theory requires interaction parameters in the form of Flory–Huggins χ parameters and Silberberg χ_W parameters, accounting for segment–segment interactions and segment–wall interactions, respectively (the usual notation for the Silberberg adsorption energy is χ_S; here we retain the subscript S for styrene units). Our choice of parameters for the present system is discussed below.

Once the segment density distributions are obtained, the refractive index profile is determined from the measured refractive index increment, dn/dc, for the polymer solution along with the quantity $dc/d\phi$. In principle, this last ratio is also experimentally accessible, but it will be treated as an adjustable parameter in this paper. This makes $dn/d\phi$ somewhat adjustable, bypassing the uncertainty from applying dn/dc, measured in dilute solution, to extreme volume fractions. We compute the Fresnel curve from the refractive index profile and compare it directly to experimental data. The effect $dc/d\phi$ has on the computed Fresnel curve is similar to the effect of changing n_1 at constant d_1 in Figure 3b.

Results

Adsorption of PS Homopolymers. We found previously that PS homopolymer did not adsorb onto glass or sapphire from the Aldrich cyclopentane solution at 23 °C.[8,9] There is, however, evidence that PS can adsorb from cyclopentane onto mica[30] and from cyclohexane onto silica.[31] We predict the density profile for 10^6 MW PS at a concentration of 10^{-4} g/mL from the self-consistent-field theory; the parameters used in the computations are given in Table II and will be discussed below in more detail. In Figure 6 we show the density profile and the corresponding reflectivity curve. It is evident from Figure 6, and from experimental reflectivity curves shown below, that the predicted change in reflectivity upon adsorption of PS is too small to observe with our reflectometer.

This negative result prompted us to measure the contact angle of water on the glass substrate with a Ramé-Hart, Inc., contact angle goniometer Model 100. Immediately after cleaning, the contact angle of the glass substrate was 18°. Subsequent exposure to a cyclopentane solution for 4 days increased the contact angle to 45°. Soaking the substrate for over 24 h in a solution of 4×10^5 PS (M_W/M_n = 1.06) at a concentration of 10^{-4} g/mL increased the contact angle to 70°. This indicates that PS can change the macroscopic surface properties and suggests its possible adsorption.

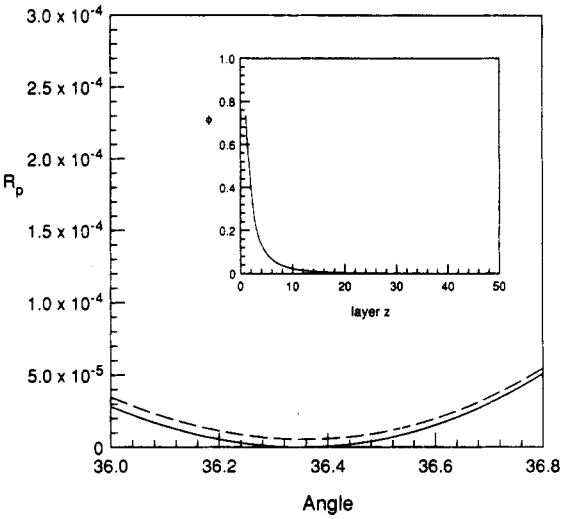

Figure 6. Reflected light intensity as a function of incident angle. The solid curve is the Fresnel interface n_0 = 1.9077 and n_1 = 1.404; the broken line is the prediction made from self-consistent-field computations for a 10^6 MW, 2000-segment, polystyrene solution at $\phi^b = 10^{-4}$. The parameters in the SCF calculations are given in Table II. In the inset the volume fraction of the adsorbed chains is given as a function of layer number.

Adsorption of PS–PEO Block Copolymers. We showed previously[8,9] that the adsorption of P170/1730 is transport limited in the concentration regime 10^{-5}–10^{-3} g/mL at shear rates up to 32 s^{-1}. In these experiments the adsorption process was monitored for about 60 min; longer observations were precluded by drift in the optical interferometer. Now, with the reflectivity approach we can monitor the adsorption process over periods of days. In Figure 7a we show the intensity of the reflected light at the Brewster angle over a period of 10 h. The results are qualitatively in line with the previous experiments. The solution at 3.5×10^{-4} g/mL initially adsorbs more swiftly than the $\sim 10^{-5}$ g/mL solution, and both curves begin to level off after approximately 1 h. Even the fact that the lower concentration reaches a higher plateau value than the higher concentration was observed before.[8,9] We proposed that the lower adsorbed amount at higher concentration was due to the fact that, above the cmc, around 10^{-4} g/mL, micelles adsorb in a random fashion effectively reducing the adsorbed amounts.[8,9] This argument assumes that the relaxation time for disintegration of the micelles is much slower than the arrival time of the polymer chains and slower than the total time of the experiment. In solution, the micelles composed of P170/1730 respond to changes in polymer concentration by changing their size within hours,[28] supporting the argument that rearrangement of adsorbed polymeric micelles requires more than 1 h. We expect that over longer periods of time the two curves shown in Figure 7a will come together or cross. In Figure 7b we show the evolution of the signal over a 3-day period. Surprisingly, the signal decays gradually, indicating that the fast initial deposition of the copolymer layer produced a nonequilibrium copolymer film. This observation might be important in surface force experiments on the same system where the

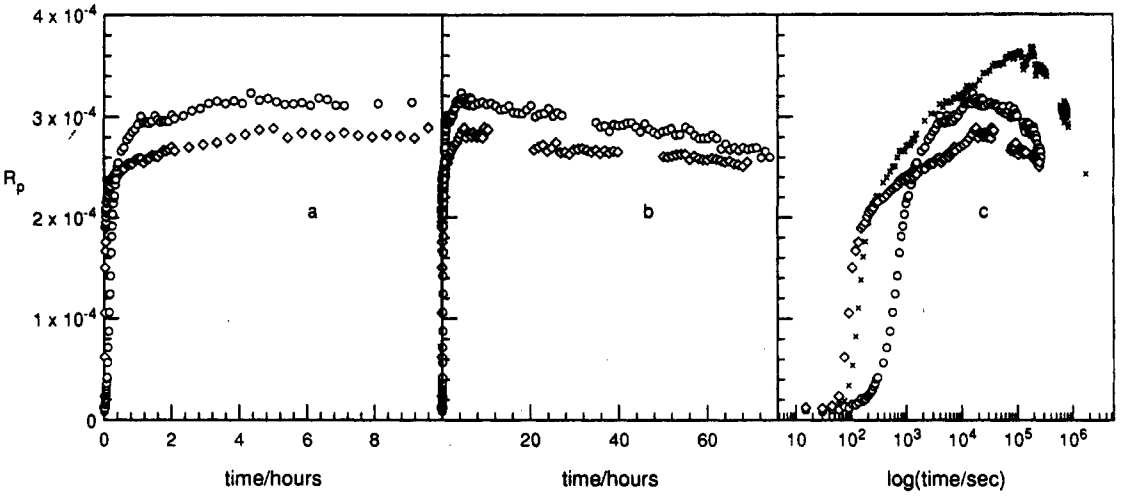

Figure 7. Reflected light intensity at a constant incident angle (36.35°) as a function of time. (a) The open circles are P170/1730, 10^{-5} g/mL solution, and the open squares ar P170/1730, 3.5×10^{-4} g/mL solution. (b) The same as in Figure 7a but on a longer time scale. (c) The same as in Figure 7b, as a function of log (time/seconds). The points indicated by × are P170/1730, 1.25×10^{-4} g/mL solution.

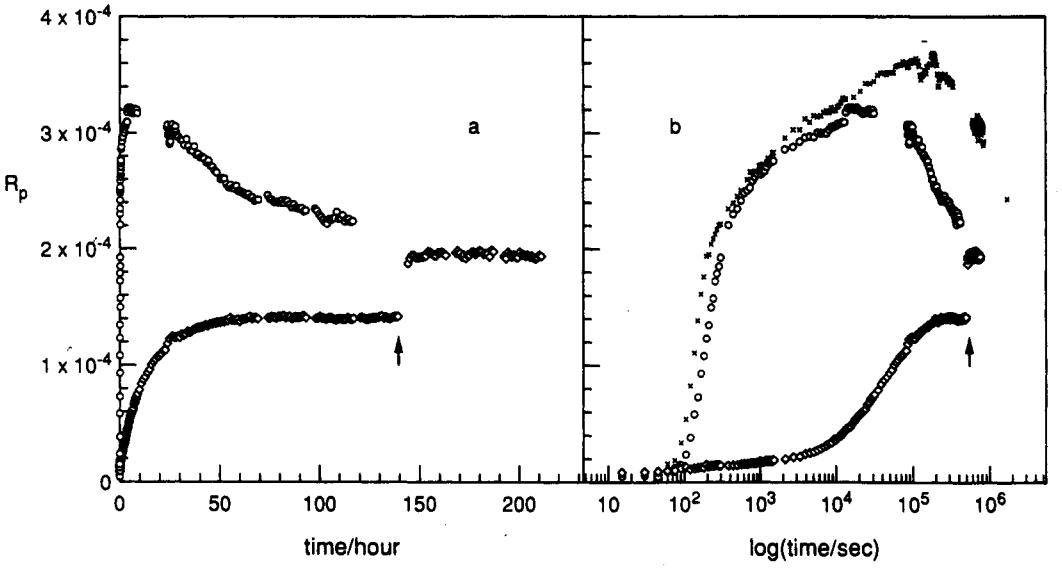

Figure 8. Intensity of the reflected light at a constant angle (36.35°) as a function of time. (a) The open circles are a P83/3470, 10^{-5} g/mL solution concentration applied to the bare surface. The open squares are a P83/3470, $<10^{-6}$ g/mL solution concentration increased to 10^{-5} g/mL at t = 140 h. (b) The same as in Figure 8a on a log (time/seconds) scale. The points indicated by × are a P170/1730, 1.25×10^{-4} g/mL solution.

adsorption process was found to be extremely fast as well.[32]

In Figure 7c we replot the reflectivity data on a log (time/second) scale. The data given in Figure 7a,b have comparable positions for the maximum in the curve; however, its magnitude depends strongly on the polymer solution concentration. We include in Figure 7c the evolution of a 1.25×10^{-4} g/mL polymer solution. We note that this concentration is between the other two, providing the first indication that an adsorbed amount is not monotonic with polymer concentration. The maximum in intensity for this solution occurs only after about 3 days, and the subsequent decay continues for 2 weeks! We will return to this change in behavior around 10^{-4} g/mL below.

Clearly there are several regimes in the adsorption process. At short times the deposition is transport limited,[8,9] subsequently, we find a transition to a regime where changes in the adsorbed layer proceed logarithmically, independent of the polymer concentration. This indicates that arrival of polymer chains at the surface is no longer rate limiting. The transition occurs when the layer is already highly populated with chains. A logarithmically slow adsorption process has been predicted recently by Johner and Joanny[33] and has been measured by Tassin et al.[7] We will discuss this point below. After the overshoot, the decay is logarithmically slow as well, suggesting that conformational changes in the layer and possibly chain desorption are rate-limiting processes.

The P83/3470 block copolymer behaves similarly as shown in Figure 8a,b for a $\sim 10^{-5}$ g/mL solution; again a fast initial rise is followed by a slow relaxation. In Figure 9a we show the typical evolution of the reflectivity curves for this case. In the first few minutes we see a shift in the apparent Brewster angle while later the curves move to higher intensity; after several days the Brewster angle retreats to lower angles. The Fresnel profiles in the first few minutes are somewhat between the limiting cases shown in Figure 3 but tend to follow Figure 3b more than Figure 3a, indicating that, in the initial deposition process, the arrival of chains is so rapid that individual chains have no time to find a more compact conformation before neighboring chains arrive at the interface. At longer times the decrease in reflected light intensity is accompanied by a shift of the apparent Brewster angle, indicating a

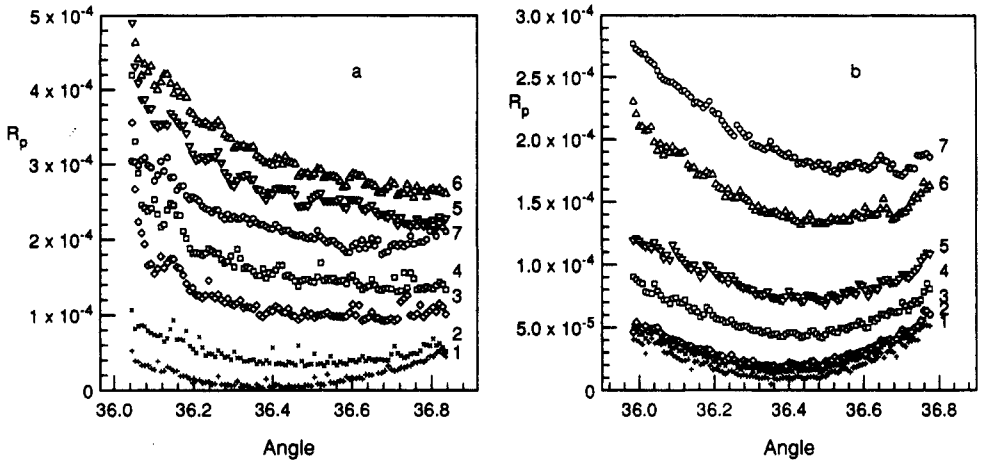

Figure 9. Intensity of the reflected light as a function of incident angle. (a) P83/3470 polymer solution at 10^{-5} g/mL at (1) t = 0, (2) t = 1 min, (3) t = 2 min, (4) t = 3 min, (5) t = 25 min, (6) t = 9 h, (7) t = 5 days. (b) P83/3470 polymer solution at $<10^{-6}$ g/mL at (1) t = 0, (2) t = 4 min, (3) t = 25 min, (4) t = 225 min, (5) t = 8 h, (6) t = 5 days, (7) t = 9 days.

reduction of the thickness of the polymer layer; however, chain desorption cannot be excluded. While this may help us to understand overall relaxations in these polymer films, it does not explain the lower adsorbed amounts observed at higher concentration.

We address this question by decreasing the initial deposition rate so that the chains may have a chance to find equilibrium conformations before subsequent chains arrive at the interface. We begin with a very low concentration, $<10^{-6}$ g/mL, of P83/3470 as shown in Figure 8a. Since the initial deposition is transport limited, we can deduce the concentration, about 5×10^{-8} g/mL, from the initial slope.[8,9] The adsorption plateau was reached within 3 days and retained for another 3 days. This stable plateau also confirms that the slow relaxation described above is not an artifact of the apparatus. We then increased the solution concentration to 10^{-5} g/mL, a concentration similar to that discussed above, and followed its adsorption for 3 days more. The layer again remained constant after reaching its new plateau value within 1 h. We believe that the layers prepared in this way are relaxed and can be compared to theoretical curves. The final signals for the 10^{-5} g/mL solution, found by the stepwise addition and by the direct adsorption to the bare surface, are in good agreement, supporting this conclusion.

In Figure 8b we present the reflected light intensity on a logarithmic time scale. The two solutions in Figure 8a are compared with the 1.25×10^{-4} g/mL solution of P170/1730 (also presented in Figure 7c). The logarithmic adsorption occurs only in the fast deposition experiments. There is no logarithmic growth for the 5×10^{-8} g/mL solution, indicating that the adsorption is transport limited. The molecular weight dependence in the logarithmic regime is surprisingly small.

It is illustrative to examine the evolution of the reflectivity curves when the molecules have time to relax their surface conformations prior to the arrival of additional chains. In Figure 9b we show that in this case the reflectivity curves follow the trend shown in Figure 3a; the layer thickens at nearly constant refractive index. This contrasts with the fast adsorption processes discussed above. We deduce from this adsorption mechanism that when the chains have time to relax, both the EO and the S units have contacts with the surface. The mechanism suggested by Figure 9b does not support a picture in which only EO segments have a favorable adsorption affinity. In this case, the layers should be thick at low coverage (on the order of twice the radius of gyration of the molecule)[14]

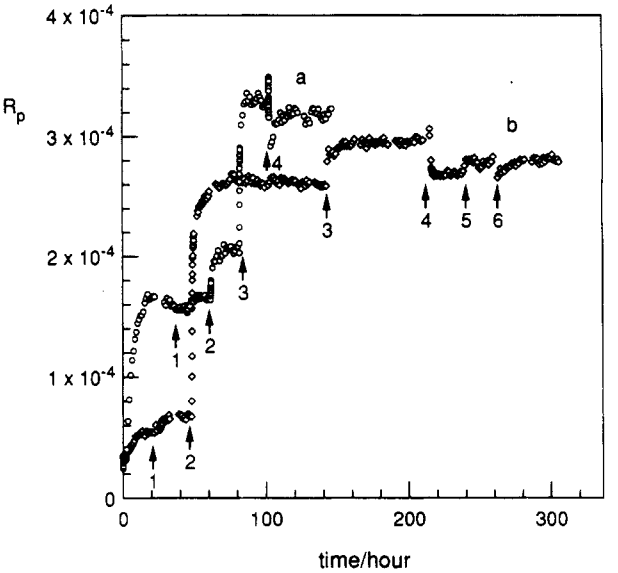

Figure 10. Intensity of the reflected light at a constant incident angle (36.35°) as a function of time: (a) P83/3470, (b) P170/1730. The arrows indicate when the solution conditions are changed. (a) (1) $\sim 5 \times 10^{-6}$ g/mL, (2) $\sim 10^{-5}$ g/mL, (3) 10^{-4} g/mL, (4) 9×10^{-4} g/mL. (b) (1) $<10^{-6}$ g/mL, (2) $\sim 4 \times 10^{-6}$ g/mL, (3) 2×10^{-5} g/mL, (4) 2×10^{-4} g/mL, (5) saturation with water, (6) 2×10^{-5} g/mL.

because the S tails have only one way to go, toward the solution.

Now that we have a method to create reproducible adsorbed layers we can study the coverage at high concentration in more detail. In Figure 10 we show two experiments conducted by a stepwise increase in the concentration of P170/1730 and P83/3470 polymers. Arrows indicate the points in time where the solutions were changed. In both experiments the initial concentrations were slightly too high, causing a small overshoot. Subsequent increases in concentration, however, produced stable layers. In the dilute regime, we find that the layers become thicker with increasing concentration; however, above a particular concentration, the signal decreases.

This observation suggests a most remarkable phenomena occurring at high chain-packing densities. The lower adsorption for the higher concentration must be considered a truly equilibrium event that we believe represents a surface phase transition. When the polymer concentration was lowered to pretransition values, the signal did not increase over a 2-day time scale, indicating that a hysteresis

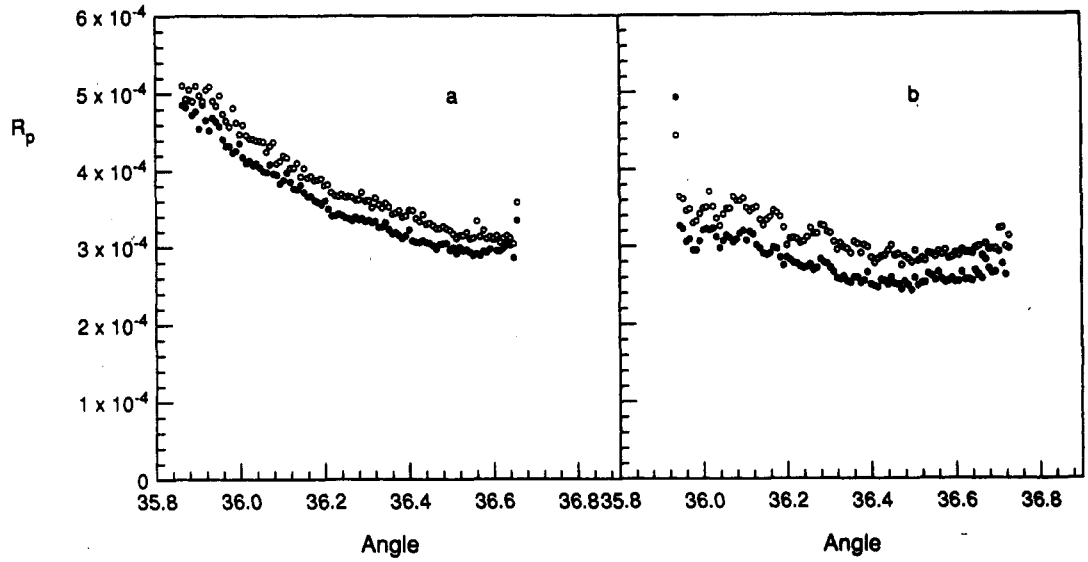

Figure 11. Intensity of the reflected light as a function of incident angle just before (open circles) and after (closed circles) the transition concentration, for the experiments shown in Figure 10: (a) P83/3470, (b) P170/1730.

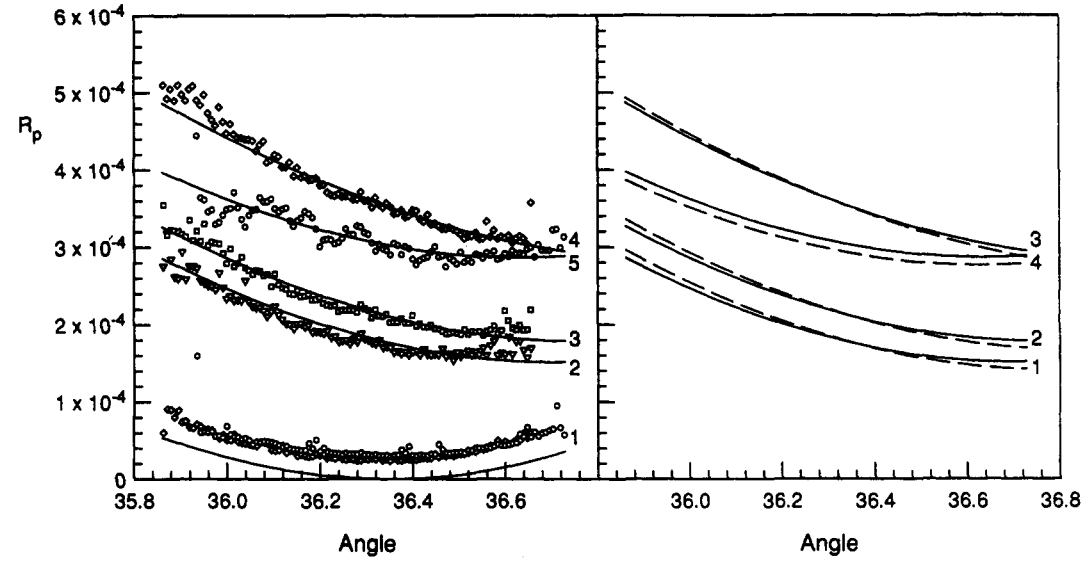

Figure 12. (a) Collection of experimental data and theoretical predictions. The intensity of the reflected light is shown against the angle of incidence. Experiments (symbols) are taken from plateau values in Figure 10. Parameters for the SCF calculations are given in Table II. (1) Experiment: $t = 0$, bare surface. Theory: Fresnel interface. (2) Experiment: P83/3470, $c = 10^{-6}$ g/mL. Theory: $E_{17}S_{680}$, $\phi^b = 4 \times 10^{-8}$. (3) Experiment: P83/3470, $c = 5 \times 10^{-6}$ g/mL. Theory: $E_{17}S_{680}$, $\phi^b = 3 \times 10^{-7}$. (4) Experiment: P83/3470, $c = 5 \times 10^{-4}$ g/mL. Theory: $E_{17}S_{680}$, $\phi^b = 5 \times 10^{-4}$. (5) Experiment: P170/1730, $c = 5 \times 10^{-5}$ g/mL. Theory: $E_{34}S_{340}$, $\phi^b = 5 \times 10^{-5}$. (b) Theoretical reflectivity curves for different choices of the model parameters. The continuous lines are $\chi_{WE} = 3.15$ and $\chi_{WS} = 1.25$: (1) $E_{17}S_{680}$, $\phi^b = 5 \times 10^{-4}$, (2) $E_{17}S_{680}$, $\phi^b = 3 \times 10^{-7}$, (3) $E_{17}S_{680}$, $\phi^b = 4 \times 10^{-8}$, (4) $E_{34}S_{340}$, $\phi^b = 5 \times 10^{-5}$. The dashed curves are for $\chi_{WE} = 2.5$ and $\chi_{WS} = 0$: (1) $E_{17}S_{680}$, $\phi^b = 6 \times 10^{-8}$, (2) $E_{17}S_{680}$, $\phi^b = 4 \times 10^{-7}$, (3) $E_{17}S_{680}$, $\phi^b = 5 \times 10^{-4}$, (4) $E_{34}S_{340}$, $\phi^b = 5 \times 10^{-5}$.

is present. In an attempt to test the stability of this transition, we added a small amount of water to saturate the cyclopentane solution. A small increase in signal was observed as the layer adjusted to the higher water background; however, it never recovered to its pretransition value, suggesting that this layer is resistent to changes in water content. In Figure 11a,b we collect the reflectivity curves just before and after the transition for both polymers. The fact that, in both cases, we observe a decrease in magnitude and in apparent Brewster angle, indicates that the layers are less extended into solution after the transition. Although the total adsorbed amount may have changed slightly, the altered layer is more compact near the surface. This is consistent with a transition from a homogeneous layer into inhomogeneous micellar-type structures on the surface where both ethylene oxide and styrene are in contact with the interface. We will discuss this interesting phenomena further below. We note that adsorbed micelles are observed in the initial rise of the adsorption isotherm[34] for small surfactants. In the surfactant case, the hydrocarbon tails drive the self-assembly near the surface while here the smaller part of the chains self-assemble; thus, the transition observed in our experiments is not related to that in surfactants.

The Fresnel curves for the various plateau values found in Figure 10 are presented in Figure 12a. There is a significant difference in the reflectivity curves for the two polymers, their shape also depending on the polymer concentration. Since the curves represent stable surface layers, theoretical modeling is opportune.

Discussion

Comparison with Self-Consistent-Field Computations. In order to compare experimental results with theoretical predictions from the self-consistent-field the-

ory, we must choose appropriate sizes for statistical segments as well as each segment–segment and segment–surface interaction energy parameter. In Table II we show the values for all the parameters; those indicated by an asterisk are chosen to fit theory to experiment but held constant for both polymers. These values are therefore determined by our experiments. The most important parameters are discussed below.

To satisfy the underlying assumption of a first-order Markov approximation used in the chain statistics (see Appendix B), one needs large statistical units; however, the assumption that all segment types and solvent molecules are of equal size, each filling a lattice site, requires small statistical segments. We choose five real segments to represent a statistical segment, irrespective of the monomer type. The length of a statistical segment implies the spacing between the layers; here we choose 1.2 nm, in accord with molecular sizes. In reference to Figure 3a, variation of this length scale has the effect of changing d_1 at constant n_1. The use of statistical segments directly effects the values for the various interaction parameters.

In the computations we neglect the presence of water in the system. We know, however, that water has a significant effect on the block copolymer micellization process[28] and will undoubtedly effect the adsorption behavior. We trust that most of these effects can be included in the energy parameters. Although all parameters are in principle measurable, until they become available we necessarily make educated choices treating them, in some sense, as adjustable parameters.

First, we must define energy parameters for segment–segment and segment–solvent interactions. Fortunately, the P170/1730 polymer has been well characterized in our laboratory. The estimated cmc, 10^{-4} g/mL,[8,9,28] pinpoints the value for $\chi_{CE} = 1.4$ (C = cyclopentane, E = ethylene oxide). Since cyclopentane is a near-Θ solvent for styrene, we choose the value $\chi_{CS} = 0.45$ (S = styrene). Finally, the interaction between S and EO must be characterized. Because few of these contacts occur, it is not a very critical parameter and is set to $\chi_{SE} = 0.5$. By definition all Flory–Huggins interaction parameters between similar segments are zero.

Second, we must account for interactions between segments and the surface via Silberberg's definition; i.e., a positive value indicates that the exchange of an adsorbed solvent molecule with a segment is energetically favorable. The $\chi_{WE} = 3.15$ is close to our previous estimate[8,9] and of the proper magnitude for ethylene oxide/SiOH bonds; $\chi_{WS} = 1.25$ is very close to the interaction parameter for styrene on silica in, for example, cyclohexane,[31] and again, by definition, $\chi_{WC} = 0$. Comparison between experiment and theory can, at best, be semiquantitative due to the number of unknown parameters. In comparing with experimental data, we focus on such aspects as the position of the apparent Brewster angle, the correct curvature, and the proper trends upon dilution.

In Figure 12a we show how well the theory predicts the large difference between the two types of polymer. It also captures the fact that the P83/3470 curves change dramatically upon dilution. Before predicted density profiles are looked at, it is interesting to investigate the sensitivity of predicted reflectivity curves to changes in model parameters. We focus on the apparent Brewster angle for P83/3470, which shifts to lower angle for lower coverages. When $\chi_{WS} = 0$ and $\chi_{WE} = 1.5$, we found a reasonable fit at higher coverage, but upon dilution the apparent Brewster angle did not decrease sufficiently, as shown in Figure 12b. With these parameters styrene has

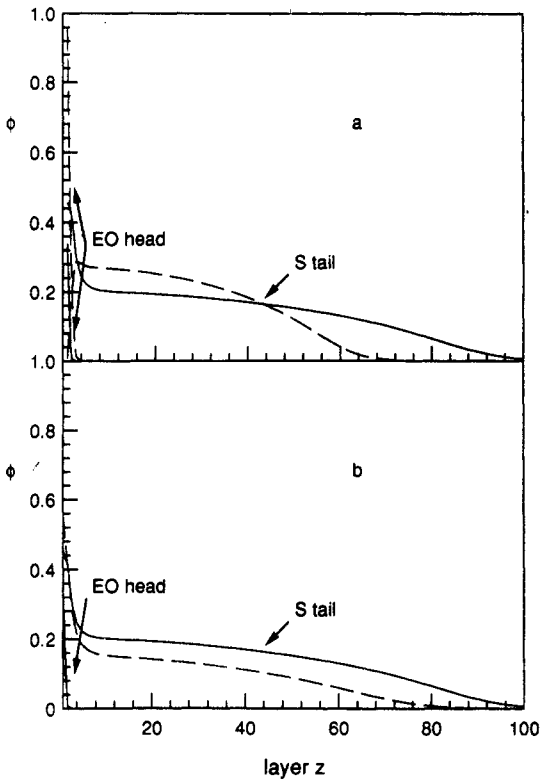

Figure 13. Segment density profiles predicted by the self-consistent-field theory. (a) The continuous curve is the profile corresponding to the theoretical reflectivity curve shown Figure 12a.4 ($E_{17}S_{680}$, $\phi^b = 5 \times 10^{-4}$); the broken curve corresponds to Figure 12a.5 ($E_{17}S_{340}$, $\phi^b = 5 \times 10^{-5}$). (b) The broken curve is the profile corresponding to 12a.2 ($E_{17}S_{680}$, $\phi^b = 4 \times 10^{-8}$). The continuous curve corresponds to Figure 12a.4 ($E_{17}S_{680}$, $\phi^b = 5 \times 10^{-4}$).

no affinity for the surface and consequently lowering the coverage reduces the chain density near the surface at constant layer thickness. The parameters from Table II better represent the data, and these density profiles will be given below.

In Figure 13 we show the predicted density profiles corresponding to the reflectivity curves in Figure 12a first, in Figure 13a comparing P83/3470 with P170/1730. As expected, virtually all the EO units are next to the surface, and with P170/1730 this first layer is almost completely filled, indicating saturating adsorbed amounts. On the other hand, the P83/3470 polymer retains PS segments in contact with the surface. The excess adsorbed amount for P83/3470, 14.16 equivalent monolayers, is slightly higher than the 13.03 for P170/1730. This corresponds to about 10 times the adsorbed amount typically found for homopolymer adsorption. The conversion factor from equivalent monolayers to milligrams per meters squared is approximately 1. The longer tail of the P83/3470 molecule extends about 50% farther into the bulk, thus diminishing the density away from the surface. Both molecules show the profile characteristic of the tails "fixed" to the surface by one end.[19] In Figure 13b we show the density profiles at a lower equilibrium concentration. As expected from the discussion above, we find the tails not to extend as far into solution while the density of styrene next to the wall increases due to the fact that at a lower coverage there are fewer ethylene oxide segments near the surface.

Finally, in Figure 14 we present the adsorption isotherms with the parameters given in Table II up to the CMC for P170/1730 and up to the maximum for the P83/3470; no micelles are found for this copolymer. Both isotherms

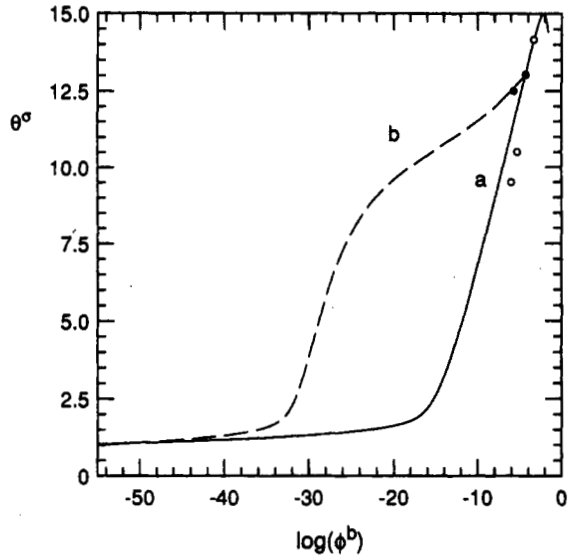

Figure 14. Excess adsorbed amount in equivalent monolayers is plotted against the logarithm of the equilibrium volume fraction. (a) P83/3470 sample: (—) theory; (○) experiment. (b) P170/1730 sample: (- - -) theory; (●) experiment.

have a "foot" at very low equilibrium concentration. The large number of styrene segments in both copolymer chains produces a high affinity adsorption isotherm (the initial rise in the isotherm is not indicated). In this regime, the density profile is very similar to that of an adsorbed homopolymer. In the next regime the adsorbed amount increases linearly with log ϕ^b as EO segments displace S segments from the surface. At very low concentration this process is already complete for the P170/1730 molecule, while for P83/3470 it continues over the entire isotherm. Since they are expressed as excess quantities (see eq 5) both isotherms will go to 0 at a $\phi^b = 1$ (not indicated in Figure 14); this is why P83/3470 has a maximum at high concentration. In Figure 14 we indicate a few experimental points for both polymers. Although the range for the measurable isotherm is small, the available data follow the predictions; for P170/1730 increasing the solution concentration alters the adsorbed amount only slightly, while for P83/3470 a significant increase in adsorbed amount is evident.

Overshoot. The overshoot phenomenon, shown very dramatically in the present system, is perhaps a fairly general problem. Chain molecules arriving at the interface must assume new conformations, a rearrangement process that can be very slow. Cohen Stuart et al. studied the rearrangements of homopolymers by measuring their hydrodynamic layer thickness in the Henry region of the adsorption isotherm as a function of time after deposition.[35] They observe that the hydrodynamic layer thickness is initially on the order of the solution coil size, subsequently collapsing to a flat conformation. The higher the concentration of polymers in the layer, the slower the rearrangement.

In general, when the surface interactions are not too strong, polymer adsorption equilibrium is within reach on a relatively short time scale; however, in polyelectrolyte systems for example strong interactions can make equilibrium more difficult to reach. An outstanding problem in polyelectrolyte adsorption is the discrepancy between theoretic expectations of a very thin adsorbed layer,[36] with the thick layers found in surface force[37] or ellipsometry[38] experiments. In light of the present discussion we can explain this dilemma. In bulk solution, the charged polyelectrolytes have very swollen conformations due to the repulsion between the segments. When the surface is of opposite charge, polyelectrolytes are strongly attracted to it. At moderate solution concentrations rearrangement becomes much slower than the characteristic time for chain arrival. Then, due to the semipermanent character of a segment–surface bond, the layer relaxation becomes very slow.

One must ask whether in the present system the slow relaxation is caused by chain rearrangements or by desorption from the surface. Since the overshoot is coupled to a very fast initial deposition, we believe that the initial layer is far from equilibrium, preventing us from answering the question with the SCF model. A maximum in adsorbed amount is thus produced as the system relaxes. In some cases the magnitude of the overshoot indicates the necessity of chain desorption. When relaxed adsorbed polymer layers are desired, the concentration step experiment, suggested in this paper, can be generally applied.

Kinetics. It is clear that the present system shows relaxation effects on very remarkable time scales; some of these observed transients have not yet been discussed in proper perspective. The fact that we must use extremely dilute polymer solutions indicates the length of the relevant relaxation time for chains arriving at a bare surface. Once a stable layer is formed and the polymer solution concentration is increased, a new plateau is reached quickly, within 1 h. This is surprisingly fast because new chains must diffuse through an already densely packed layer to the surface. These changes in the adsorbed layer upon variation of solution conditions show that, although the chain packing is high, the layer must be considerably mobile. The high mobility can also explain the rate at which the polymer layer goes through its phase transition, again on a 1-h time scale.

Having concluded that the diffusion process through the brush layer is relatively fast, we exclude this from the logarithmically slow adsorption phenomena found in relation to the overshoot. The fact that we find a negligible molecular weight dependence in the logarithmic regime supports this conclusion. We believe that the adsorbing part of the block copolymer is responsible for the slow kinetics. It is known that ethylene oxide can crystallize,[39] and although it is difficult to imagine a real crystal forming near the surface, cooperative ordering effects can explain the slow relaxations. One can also argue that, near the surface, chains can be in a glassy state created by the locally high segment density. This phenomenon supports the slow relaxation process, but it cannot explain why some rearrangements in the layer, for example, the ones related to the phase transition, are relatively fast.

Surface Phase Transition. There is ample evidence for a surface phase transition. In the concentration step experiments the intensity of the reflected light at the Brewster angle drops when the solution concentration exceeds a given value. In addition, there are significant differences in the reflectivity curves below and above the transition concentration, and there is a dramatic concentration dependence in the fast deposition experiments at times comparable to the beginning of the relaxation process in the overshoot. The calculations shown above do not predict a surface phase transition; the adsorbed amounts increase with the bulk concentration. If the transition is characterized by the creation of lateral inhomogeneities in the layer, as suggested above, the calculations will not show this due to the local mean-field approximation. We believe the surface phase transition appears as presented in Figure 15. Rather than being next to the surface, some of the EO chain parts begin to group together, forming

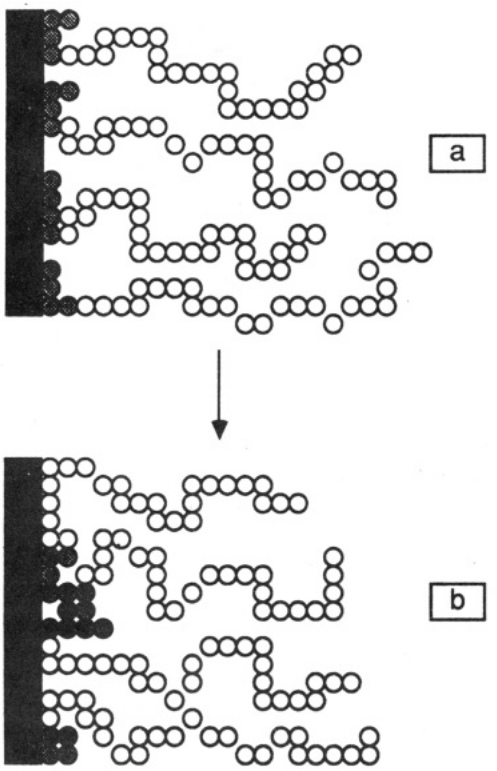

Figure 15. Block copolymers composed of 4 EO units and 25 S units adsorbed at the surface. (a) Prior to the phase transition, almost all of the EO segments contact the surface; the styrene chains protrude far into solution. (b) After the phase transition, EO units are now grouped together in aggregates and S segments are in contact with the contact with the surface and the S tails do not extend as far into solution.

local structures that are micellar in nature. The tails pointing toward the solution may have in fact more space available from the local curvature. We hypothesize that, at high chain densities, the EO units gain considerable energy when they self-associate rather than forming favorable bonds with the surface. In other words, the EO units may need a specific orientation to gain energy from a surface contact, and if this orientation is not possible at high densities, the energy balance is altered. This association and ordering argument may shift the balance of surface forces toward the initiation of lateral inhomogeneities described above. Preliminary computations with a two-dimensional version of the self-consistent-field theory, which can handle lateral inhomogeneities, show that surface micelles are possible for these asymmetric molecules when the adsorption energy for the two segment types in the chain are of the same magnitude. In the unlikely event that we have overestimated the difference in adsorption affinities in our analysis, we do not need the cooperative ordering argument used above to explain the transition. We believe that the phase transition discussed above is due to self-assembly of the copolymer chains and will therefore occur only with amphiphilic molecules in a selective solvent where a number of conditions such as a proper balance between surface forces and the molecular compositions are satisfied.

Conclusions and Summary

We have presented a dynamic scanning angle reflectometer well suited for the study of block copolymer adsorption for a number of reasons. First, the block copolymer layers are very thick, and thus the intensity of the reflected light is easily measurable with a photodiode array. Second, the apparatus is very stable in time so that the slow adsorption, desorption, and rearrangement processes can be followed. Third, the reflectivity curves show considerable variation upon changes in surface coverage and profile, and thus the apparatus gives insights in the structure of the polymer layer and its evolution in time.

We found that under normal conditions highly asymmetric copolymers with a small ethylene oxide and large styrene blocks adsorb rapidly on a glass surface from a cyclopentane solution; a high coverage is often reached within hours. Under these conditions, however, a relaxation process is observed. The initial deposition rate of chains onto the surface is faster than the time required for a chain to find its optimal conformations. This leads, in general, to thick layers, on the order of 75 nm, far from equilibrium and a possible excess of chains on the surface. The rearrangements or desorption of chains from this thick polymer layer are very slow, occurring over periods of days or weeks.

We propose a concentration step experiment to overcome this problem. In this experiment, an extremely dilute polymer solution is brought in contact with the surface. The overshoot and relaxation is now absent since the deposition rate is very much reduced and the chains rearrange upon arrival before subsequent molecules fill the surface. After the adsorption of this solution is completed, the concentration is increased stepwise to the desired value. In this way stable adsorbed layers approaching equilibrium are prepared. This concentration step strategy can be useful in other polymer adsorption systems, such as polyelectrolytes, where nonequilibrium segment density profiles are likely to form.

We were not able to increase the surface coverage of P170/1730 above 13 mg/m^2 and of P83/3470 above 14 mg/m^2. Any attempt to increase the number of adsorbed chains by increasing the solution concentration resulted in a surface phase transition characterized, most likely, by laterally inhomogeneous density profiles. We hypothesize an ordering of the ethylene oxide chains causes a change in the balance between surface interaction forces, increasing the likelihood that styrene units are found near the surface while the ethylene oxide units reside in localized regions on or near the surface. These micellelike structures cause the local density in the first 5–10 nm near the surface to increase and the total layer thickness to decrease because the styrene segments can form more contacts with the surface.

We model the adsorbed copolymer layers, below the phase-transition concentration, with the self-consistent-field theory of Scheutjens and Fleer. We convert predicted segment density profiles into refractive index profiles and reflectivity curves using the matrix method of Abelès. Reasonable choices for the model parameters produce semiquantitative agreement for the variation with both molecular composition and adsorbed amounts. The theoretical density profiles show ethylene oxide units in a flat conformation near the wall, while the styrene units protrude far into solution. From the model we learn than styrene has a favorable interaction with the surface when adsorbed from cyclopentane but that it is easily displaced by ethylene oxide segments.

The adsorption kinetics suggest that diffusion of chains through the brush layer is relatively fast, implying that the chains within the layer are quite mobile. In experiments where the chains are rapidly deposited on the surface, subsequent logarithmically slow rearrangement processes indicate a slow relaxation of the high density of ethylene oxide near the surface. It is not likely that this ethylene oxide layer is in a glassy state. We believe,

however, that cooperative ordering effects of EO near the surface contribute to the prohibitively long relaxation times. We are currently investigating this in experiments with amorphous diblock copolymers.

Acknowledgment. This work is supported by du Pont Marshall Laboratories and by an IBM Faculty Development Award. Many thanks go to Bob Tilton for his help in the all-night adsorbatorium, to Mark Munch for his advice in the early stages of this work, and to David Marr for his careful reading of this paper.

Appendix A. Reflection of Polarized Light from Stratified Isotropic Planar Layers[4]

Consider a stratified interface composed of many parallel layers $z = 1, ..., M$ each of thickness d_z and with an isotropic refractive index n_z. Both for $z < 1$ and for $z > M$ the refractive index is homogeneous throughout. The transmitted direction (to higher z) is indicated by a superscript while reflected direction is indicated by a superscript minus. An incident parallel polarized wave of light (the superscript p is dropped) in the medium 0 generates a reflected wave in 0 and a transmitted wave at $M + 1$. In vector notation the total field at a plane z is

$$\mathbf{E}(z) = \begin{bmatrix} E^+(z) \\ E^-(z) \end{bmatrix} \tag{A1}$$

A 2×2 scattering matrix S relates the field between the planes at z and z', $\mathbf{E}(z) = \mathbf{S}\mathbf{E}(z')$. The total scattering matrix, i.e., the one relating the light wave in medium 0 and the light on the other side of the interface ($z = M + 1$), is thus

$$\begin{bmatrix} E^+(0) \\ E^-(0) \end{bmatrix} = \begin{bmatrix} S_{11} & S_{12} \\ S_{21} & S_{22} \end{bmatrix} \begin{bmatrix} E^+(M+1) \\ 0 \end{bmatrix} \tag{A2}$$

The relative intensity of the reflected light is given by $R = S_{21}/S_{11}$. The scattering matrix is composed of two types of matrices called the interface matrix, $\mathbf{I}$, and the layer matrix, $\mathbf{L}$. The first one handles the reflection and refraction of the light passing through the step in refractive index between two consecutive layers, while the second matrix accounts for the phase shift of the light traveling through the layer. Thus in this case

$$\mathbf{S} = \mathbf{I}_{01} \prod_{z=1}^{M} \mathbf{L}_z \mathbf{I}_{z(z+1)} \tag{A3}$$

the interface matrix is a function of the interface Fresnel reflection (see eq 2)

$$\mathbf{I}_{zz'} = \begin{bmatrix} 1 & r_{zz'} \\ r_{zz'} & 1 \end{bmatrix} \tag{A4}$$

and the layer matrix is given by

$$\mathbf{L}_z = \begin{bmatrix} e^{j\beta_z} & 0 \\ 0 & e^{-j\beta_z} \end{bmatrix} \tag{A5}$$

where the film phase thickness, β_z, is given in the text (eq 3). Finally, the angle with respect to the normal is found by applying Snell's law. These equations provide a means to calculate the reflectivity for an arbitrary layered refractive index profile.

Appendix B. Self-Consistent-Field Theory for Polymer Adsorption[20-24]

The volume fraction of segment s of chain type k in layer z (segment probability amplitude) is related to the product of the chain end distribution function computed by starting at segment number 1, $G_k(z,s|1)$, and the chain end distribution function starting at segment number r, $G_k(z,s/r)$, as

$$\phi_k(z,s) = C_k \frac{G_k(z,s|1)\, G_k(z,s|r)}{G_k(z,s)} \tag{B1}$$

where C_k is a normalization calculated from either the bulk volume fraction of molecule k

$$C_k = \phi_k^{\,b}/r_k \tag{B2}$$

or, when the number of molecules in the system, normalized by the number of lattice sites in a layer, $\theta_k = \sum_z \sum_s \phi_k(z,s)$, is known from

$$C_k = \frac{\theta_k}{r_k \sum_z G_k(z,r|1)} \tag{B3}$$

In eq B1 the division of $G_k(z,s)$ is performed to correct for double counting of the overlapping segments of rank s. A simple recurrence formula relates the chain end distribution function, $G_k(z,s|1)$, to that for a chain one segment shorter as

$$G_k(z,s|1) = \langle G_k(z,s-1|1) \rangle\, G_k(z,s) \tag{B4}$$

A similar equation holds for the chain end distribution functions started from the opposite end of the molecule. The broken brackets in eq B4 indicate a weighted average over three layers $z - 1$, z, and $z + 1$ for $z > 1$ and over two layers for $z = 1$

$$\langle G(z) \rangle = \lambda_{-1} G(z-1)(1 - \delta_{z1}) + \lambda_0 G(z) + \lambda_1 G(z+1) \tag{B5}$$

where λ_{-1}, λ_0, and λ_1 are a priori probabilities to move to a previous layer, to stay in the layer, or to step to a following layer in the lattice, respectively. In a hexagonal lattice these values are 0.25, 0.5, and 0.25, respectively. Note that the use of eq B4 implies that the history of the chain trajectory is only one segment long, corresponding to a first-order Markov approximation. Since $G_k(z,1|1) = G_k(z,1)$, the problem is solved when the free segment distribution functions, $G_k(z,s)$ are known. If segment s of molecule k is of type x, we have $G_k(z,s) = G_x(z)$. It can be shown that $G_x(z)$ is given by a Boltzmann equation

$$G_x(z) = e^{-u_x(z)/kT} \tag{B6}$$

where $u_x(z)/kT$ is the local mean-field potential a segment type x "feels" in layer z. The general formula for this potential

$$u_x(z) = u'(z) + kT \sum_y \chi_{xy} (\langle \phi_y(z) \rangle - \phi_y^{\,b}) - kT \chi_{W_x} \delta_{z1} \tag{B7}$$

includes a Lagrange parameter, $u'(z)$, coupled to the condition that all lattice sites must be filled, i.e., incompressibility

$$\sum_x \phi_x(z) = 1 \tag{B8}$$

Physically $u'(z)$ is a hard-core repulsion. The second term in eq B7 represents all possible segment–segment interactions and is properly normalized with respect to the interactions in the bulk. The broken brackets have the same meaning as those in eq B5. The third term accounts for the interaction of segment x with the surface, only in effect of course when the segment x is in layer 1. The

minus sign in front of the third tem of eq B7 is a consequence of the Silberberg adsorption energy definition.

The set of equations is closed. In each layer the unknown Lagrange parameter $u'(z)$ is coupled to eq B8, and for each segment type in each layer, the unknown volume fraction is coupled to a potential given in eq B7. Solving these implicit equations for the volume fractions and for the value of the Lagrange parameter in each layer is, in general, only possible with use of numerical methods.[40]

References and Notes

(1) Napper, D. H. *Polymeric Stabilization of Colloidal Dispersions*; Academic Press: London, 1983.
(2) Berne, B. J.; Pecora, R. *Dynamic Light Scattering*; Wiley: New York, 1976.
(3) Elias, H. G. *Light Scattering from Polymer Solutions*; Huglin, M. B., Ed.; Academic Press: London, 1972.
(4) Azzam, R. M. A.; Bashara, N. M. *Ellipsometry and Polarized Light*; North-Holland: Amsterdam, 1977.
(5) Takahashi, A.; Kawaguchi, M. *Adv. Polym. Sci.* **1982**, *46*, 3.
(6) Lee, J. J.; Fuller, G. G. *J. Colloid Interface Sci.* **1985**, *103*, 569.
(7) Tassin, J. F.; Siemens, R. L.; Tang, W. T.; Hadziioannou, G.; Swalen, J. D.; Smith, B. A. *J. Phys. Chem.* **1989**, *93*, 2106.
(8) Munch, M. R.; Gast, A. P. *J. Chem. Soc., Faraday Trans.* **1990**, *86*, 1341.
(9) Munch, M. R.; Gast, A. P. *Macromolecules* **1990**, *23*, 2313.
(10) Schaaf, P.; Déjardin, P.; Schmitt, A. *Rev. Phys. Appl.* **1985**, *20*, 631.
(11) Schaaf, P.; Déjardin, P.; Schmitt, A. *Langmuir* **1987**, *3*, 1131.
(12) Schaaf, P.; Déjardin, P. *Colloids Surf.* **1988**, *31*, 89.
(13) Alexander, A. *J. Phys.* **1977**, *38*, 983.
(14) de Gennes, P.-G. *Macromolecules* **1980**, *13*, 1069.
(15) Patel, S.; Tirrell, M.; Hadziiouannou, G. *Colloids Surf.* **1988**, *31*, 157.
(16) Marques, C.; Joanny, J. F.; Leibler, L. *Macromolecules* **1988**, *21*, 1051.
(17) Marques, C.; Joanny, J. F. *Macromolecules* **1989**, *22*, 1454.
(18) Munch, M. R.; Gast, A. P. *Macromolecules* **1988**, *21*, 1366.
(19) Cosgrove, T.; Heath, T.; Van Lent, B.; Leermakers, F. A. M.; Scheutjens, J. M. H. M. *Macromolecules* **1987**, *20*, 1692.
(20) Van Lent, B.; Scheutjens, J. M. H. M. *Macromolecules* **1989**, *22*, 1931.
(21) Evers, O. A.; Scheutjens, J. M. H. M.; Fleer, G. J. *Macromolecules*, in press.
(22) Scheutjens, J. M. H. M.; Fleer, G. J. *J. Phys. Chem.* **1979**, *83*, 1619.
(23) Scheutjens, J. M. H. M.; Fleer, G. J. *J. Phys. Chem.* **1980**, *84*, 178.
(24) Scheutjens, J. M. H. M.; Fleer, G. J. *Macromolecules* **1985**, *18*, 1882.
(25) Leermakers, F. A. M.; Scheutjens, J. M. H. M. *J. Chem. Phys.* **1988**, *89*, 3264.
(26) Cohen Stuart, M.; Cosgrove, T.; Vincent, B. *Adv. Colloid Interface Sci.* **1986**, *24*, 143.
(27) Kim, M. W.; Peiffer, D. G.; Chen, W.; Hsiung, H.; Rasing, Th.; Shen, Y. R. *Macromolecules* **1989**, *22*, 2682.
(28) Cogan, K. A.; Gast, A. P. *Macromolecules* **1990**, *23*, 745.
(29) Hager, B. L., Berry, G. C., Tsai, H. H. *J. Polym. Sci., Polym. Phys. Ed.* **1987**, *25*, 387. Deschamps, H.; Leger, L. *Macromolecules* **1986**, *19*, 2760. Brown, W. *Macromolecules* **1986**, *19*, 387. Munch, J.-P.; Hild, G.; Candau, S. *Macromolecules* **1983**, *16*, 71.
(30) Hu, H. W.; Van Alsten, J.; Granick, S. *Langmuir* **1989**, *5*, 270.
(31) Van der Beek, G. P.; Cohen Stuart, M. A.; Fleer, G. J.; Hofman, J. E. *Langmuir* **1989**, *5*, 1180.
(32) Taunton, H. J.; Toprakcioglu, C.; Fetters, L. J.; Klein, J., to be submitted for publication.
(33) Johner, A.; Joanny, J. F., in press.
(34) Levitz, P.; Van Damme, H.; Keravis, D. *J. Phys. Chem.* **1986**, *90*, 1302.
(35) Cohen Stuart, M.; Tamai, H. *Langmuir* **1988**, *29*, 329.
(36) Evers, O. A.; Fleer, G. J.; Scheutjens, J. M. H. M.; Lyklema, J. *J. Colloid Interface Sci.* **1986**, *111*, 446.
(37) Klein, J. *J. Colloid Interface Sci.* **1986**, *111*, 2.
(38) Killmann, E.; Eckart, R. *Makromol. Chem.* **1970**, *132*, 239.
(39) Lotz, B.; Kovacs, A. J. *Kolloid-Z.* **1966**, *209*, 97.
(40) Leermakers, F. A. M.; Scheutjens, J. M. H. M. *J. Chem. Phys.* **1988**, *89*, 3264.

Registry No. (Ethylene oxide)(styrene) (block copolymer), 107311-90-0; cyclopentane, 287-92-3.